Supplementary Information to

Metastable redox-active ions as furtive n-doping agents for hybrid perovskites

*Zuzanna Molenda [a, c], Bastien Politi [b], Raphaël Clerc [b], Mamatimin Abbas [a], Sylvain Chambon [a], Dario M. Bassani [c] *and Lionel Hirsch [a] **

Zuzanna Molenda, Mamatimin Abbas, Sylvain Chambon, Lionel Hirsch

Univ. Bordeaux, CNRS, Bordeaux INP, IMS, UMR 5218, F-33400 Talence, France

E-mail : lionel.hirsch@ims-bordeaux.fr

Bastien Politi, Raphaël Clerc

Université de Lyon, Université Jean Monnet-Saint-Étienne, CNRS, Institut d'Optique Graduate School, Laboratoire Hubert Curien, UMR 5516, F-42023 Saint-Etienne, France

Dario M. Bassani

Univ. Bordeaux, CNRS, Bordeaux INP, ISM UMR 5255, F-33400 Talence, France

E-mail: dario.bassani@u-bordeaux.fr

Conductance

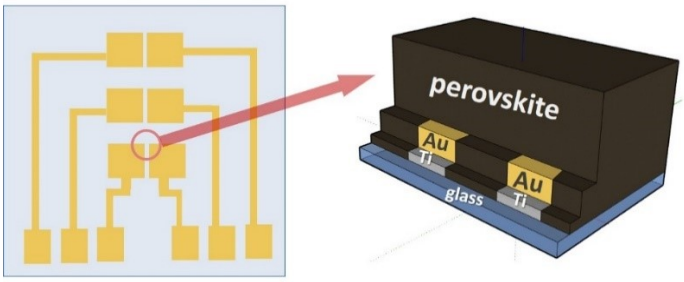

Figure S1: The sample architecture for the conductivity measurement with the top view on the left and cross section on the right.

Conductance was measured between two symmetric Ti/Au electrodes (10 and 50 nm thick, respectively), deposited through a shadow mask on the glass substrates using the electron beam evaporator. The distance between the electrodes is 200 µm and the electrode side length is 2.5 mm. The perovskite samples were spin coated on top of the electrodes.

Higher doping concentrations

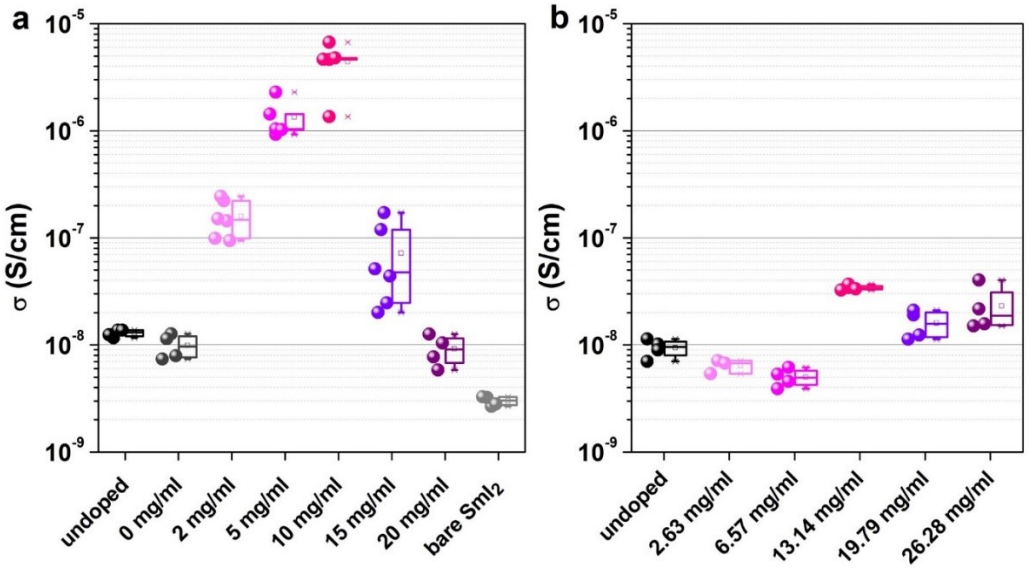

Figure S2. Conductivity of MAPI doped with 2-20 mg/mL SmI_2 and respective molar concentrations or SmI_3.

Figure S2 shows the conductivity of MAPI upon the doping concentration of SmI_2 up to 20 mg/mL (a) and respective molar concentrations of SmI_3 (b). Doping with SmI_2 of the concentration 15 and 20 mg/mL lead to a decrease of conductivity with respect to the sample 10 mg/mL. Doping with SmI_3 does not impact the conductivity in a significant way in the whole range of concentrations.

Other perovskite formulations

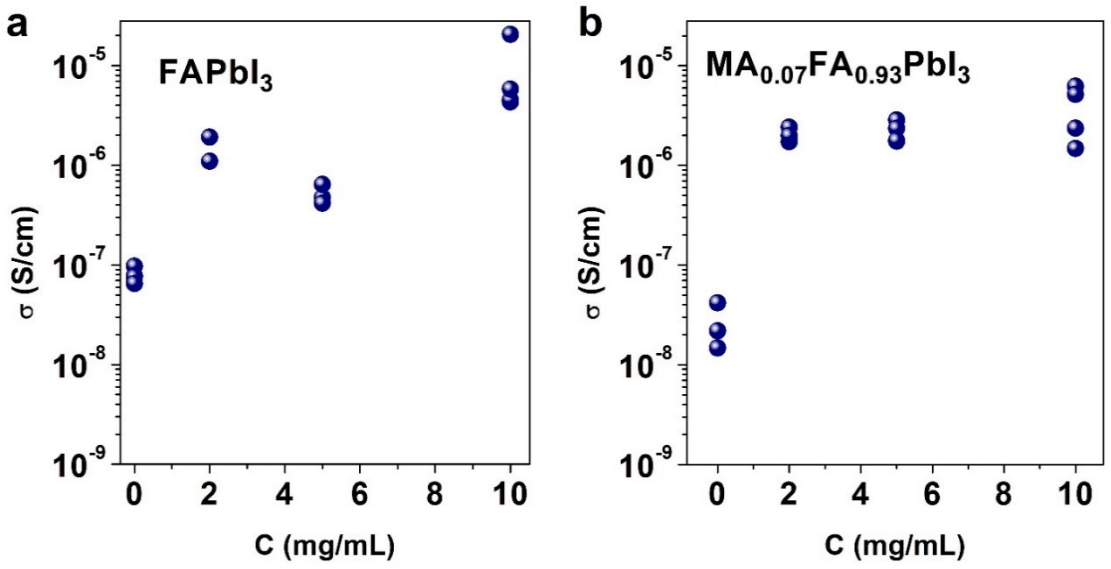

Figure S3. Conductivity of Sm-doped $FAPbI_3$ and $MA_{0.07}FA_{0.93}PbI_3$ as a function of the doping concentration.

Formamidinium iodide (FAI) and methylammonium iodide (MAI) were purchased from GreatCell Solar. All the other precursors and solvents were purchased from Sigma Aldrich.

The solutions of $FAPbI_3$ and $MA_{0.07}FA_{0.93}PbI_3$ were prepared by dissolving 1 mmol FAI and PbI_2 or 0.07 mmol MAI, 0.93 mmol FAI and 1 mmol PbI_2 in DMF:DMSO solution with the volume ratio 9:1. For the solution of $MAPbBr_3$, MABr and $PbBr_2$ were used in the same concentration. The solutions were stirred at 60°C for 2h, filtered with 0.45μm PTFE filter and spin coated at 6000 rpm for 60 s, resulting in the ~300 nm thick films. Five seconds after the spinning had begun, 0.5 mL of chlorobenzene was added. The samples were annealed at 100°C for 30 min.

The two-step doping with SmI_2 was performed as in case of MAPI.

ToF SIMS and depth-resolved XPS

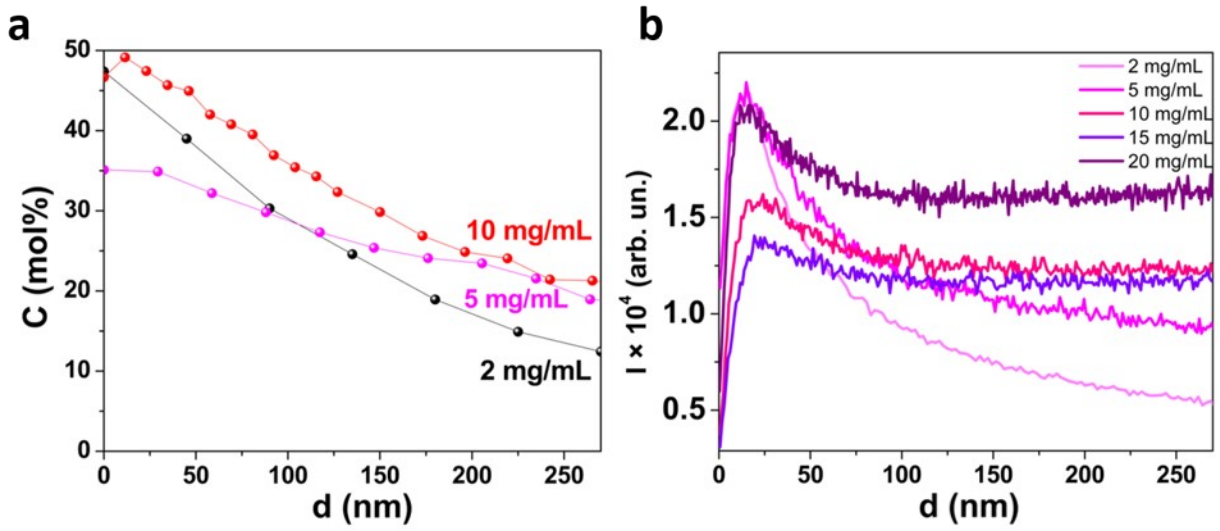

Figure S4. a) XPS Sm depth profile obtained using surface sputtering by Ar clusters, b) ToF-SIMS profiles of Sm for different doping concentrations.

Using both XPS and ToF-SIMS, it was shown that Sm is present throughout the layer, with the increased amount close to the surface, which is consistent with the doping method. The dopant density at the bottom of the layer for the sample "10 mg/mL" is around 2×10^{20} cm^{-3}, considering that the Pb density in MAPI is ~ 10^{21} cm^{-3}.

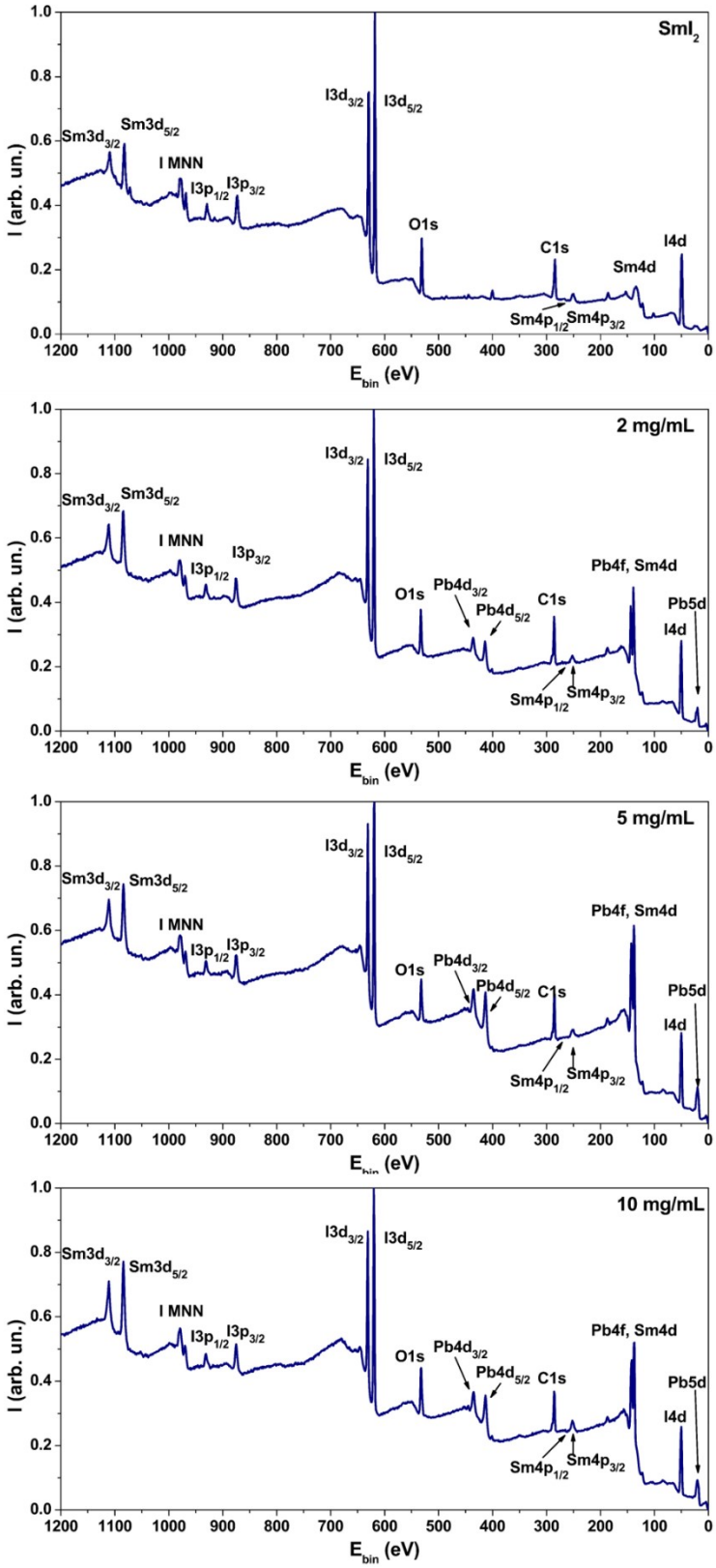
SmI2
I (arb. un.)
Ebin (eV)
Sm3d3/2
Sm3d5/2
I MNN
I3p1/2
I3p3/2
I3d3/2
I3d5/2
O1s
C1s
Sm4d
Sm4p1/2
Sm4p3/2
I4d
2 mg/mL
Pb4d3/2
Pb4d5/2
Pb4f, Sm4d
Pb5d
5 mg/mL
10 mg/mL

Figure S5. XPS survey spectra for SmI_2 layer and for MAPI doped with 2, 5 and 10 mg/mL SmI_2 solution. The presence of all the signature elements for MAPI, as well as the dopant, is observed and marked on the spectra.

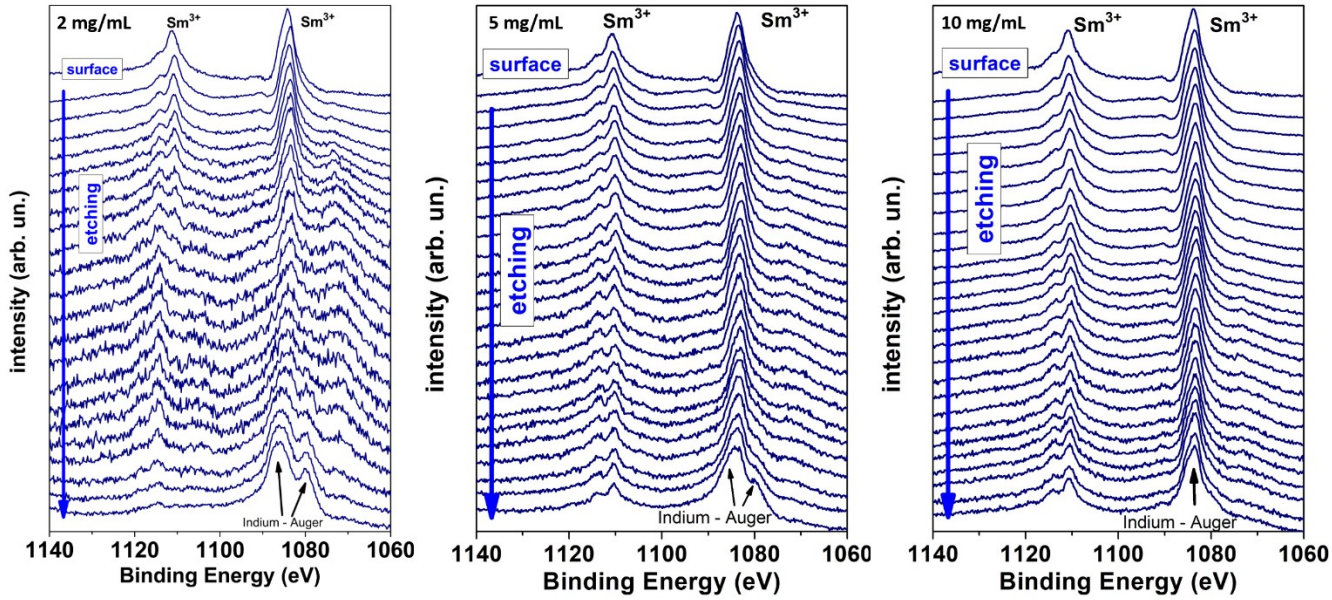

Figure S6. XPS depth profiles of Sm $3d_{5/2}$ for three different doping concentrations.

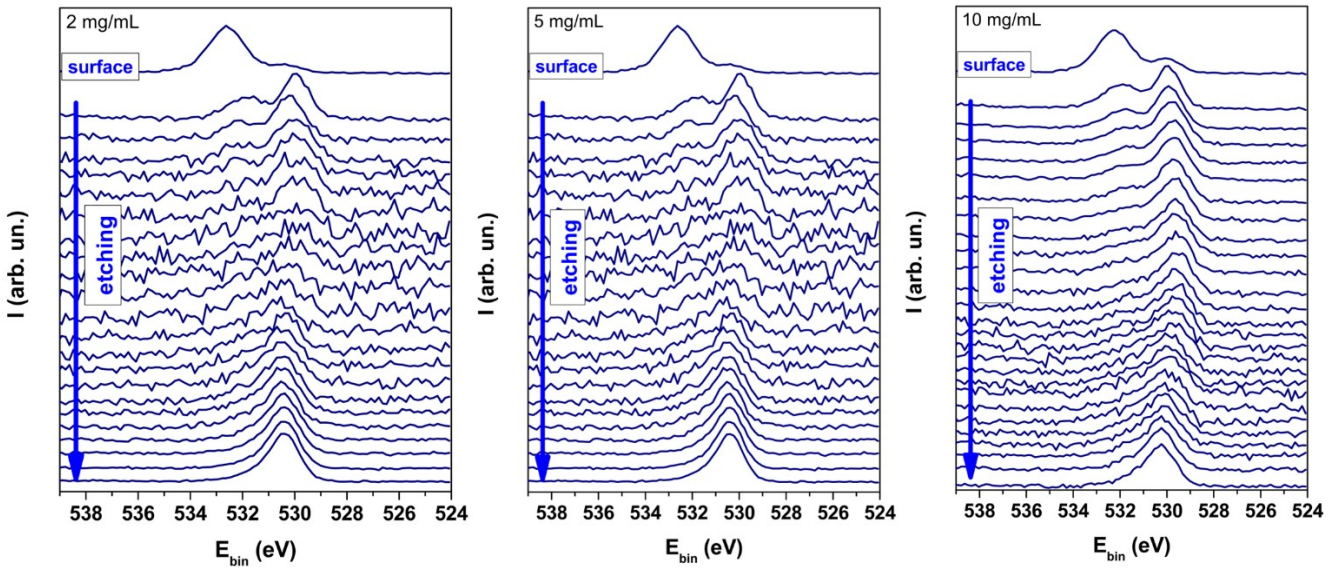

Figure S7. XPS depth profiles of O 1s for three different doping concentrations.

Both on the surface and inside the perovskite layer, the XPS peak corresponding to Sm^{3+} is found (Figure S6). Additionally, in the bulk of the layer one can notice small signals corresponding to Sm^{2+}, suggesting that some part of Sm^{2+} remains unoxydized. However, in the surface region, only the oxidized form Sm^{3+} is present. That is probably due to the oxide formation (Sm_2O_3), as it corresponds with the depth profiles of O 1s (Figure S7). On the very surface, the O 1s spectral line is characteristic for H_2O or C-O bonding from the solvent or solvent vapors present in the glovebox, that could adsorb to the surface[1]. The spectra in Figure 2 come from the layer depth of ~200 nm, as a negligible amount of oxygen can be found there, therefore we can rule out that the Sm spectra comes from Sm_2O_3. Therefore, the shift of the Sm^{3+} between the SmI_2 and perovskite doped layers may correspond to the substitution of Pb^{2+} by Sm^{3+} ions.

AFM

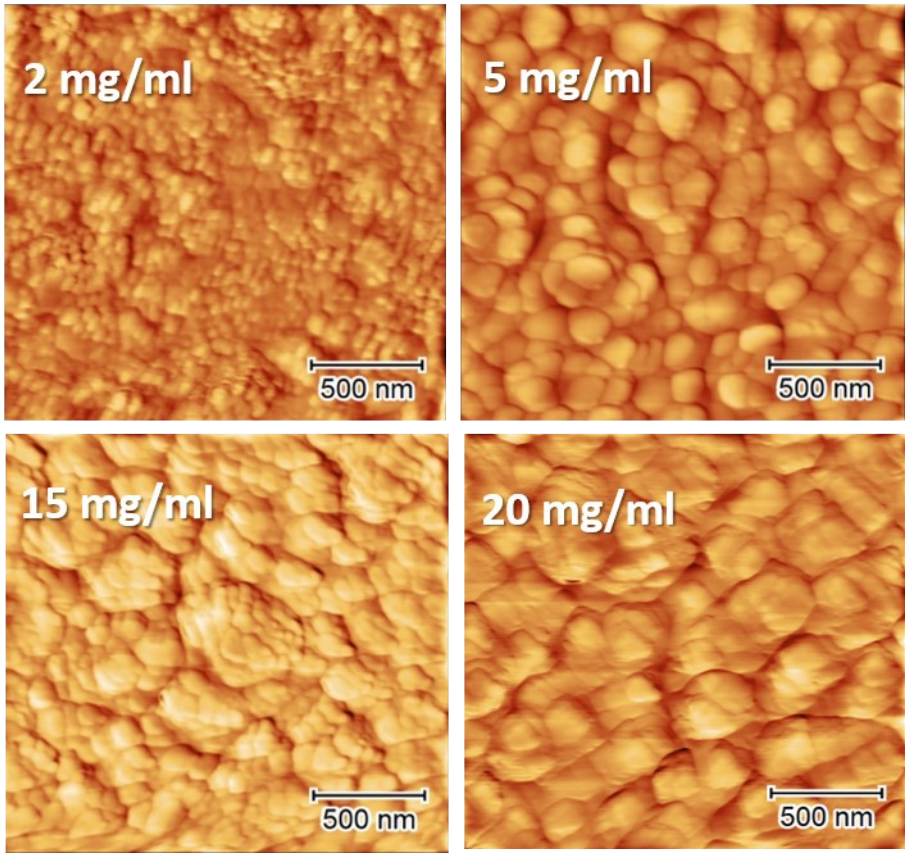

Figure S8: AFM images of MAPI doped with 2, 5, 15 and 20 mg/ml SmI_2.

The surface of all the doped samples altered upon doping and the formation of grains with the size ranging from 50 to 200 nm is observed.

XRD

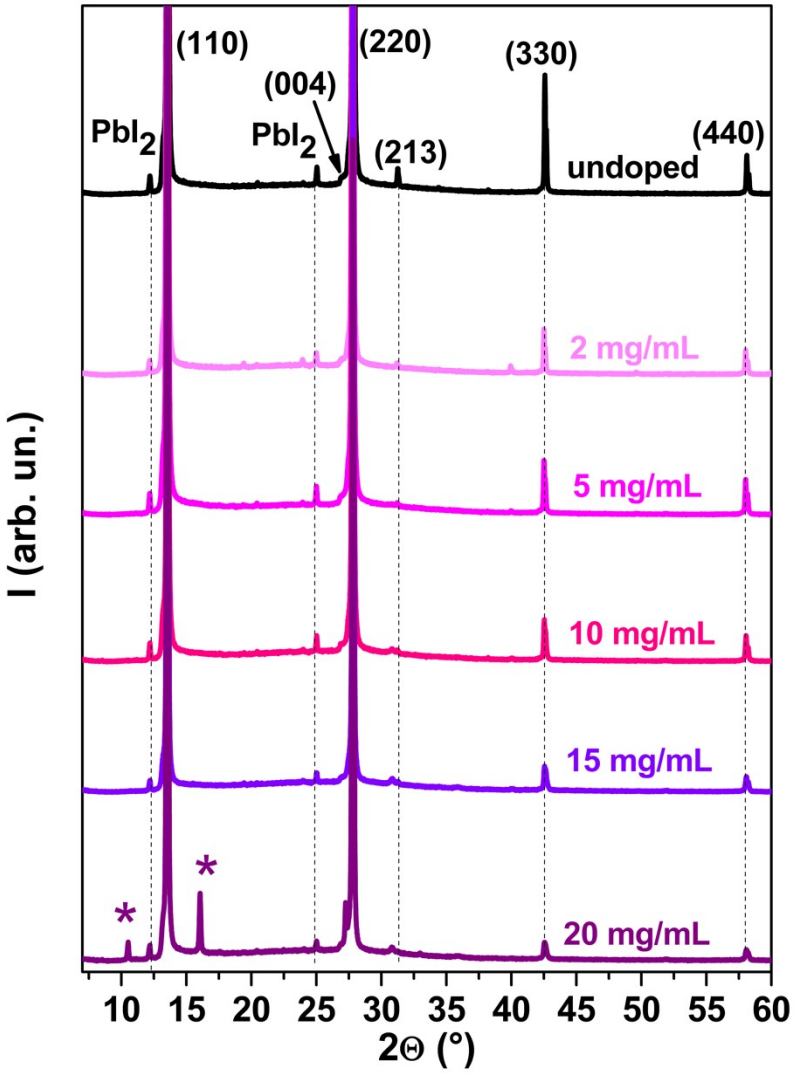

Figure S9. XRD pattern or undoped MAPI and doped with the SmI_2 concentrations 2-20 mg/mL.

For the highest doping concentration (20 mg/mL) two more peaks are present, at 10.5° and 16.0° (marked by asterisks), that do not appear for other doping concentrations. They are presumed to originate from the phase separation of the SmI_3 at grain boundaries, which might be the reason for the decreased conductivity observed at high doping concentration, as the inclusion of an insulating phase in the perovskite layer leads to a charge mobility decrease.

UV-Vis absorption spectroscopy

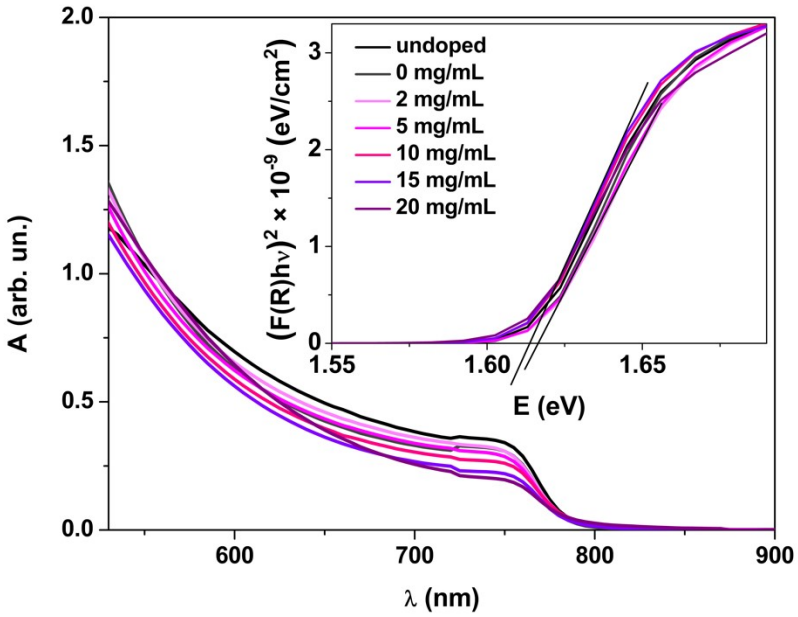

Figure S10. UV-visible absorption spectra for undoped and doped perovskite thin films. The inset presents the Tauc plots for these samples. The optical bandgap remains independent of the doping concentration.

Surface potential difference using KP

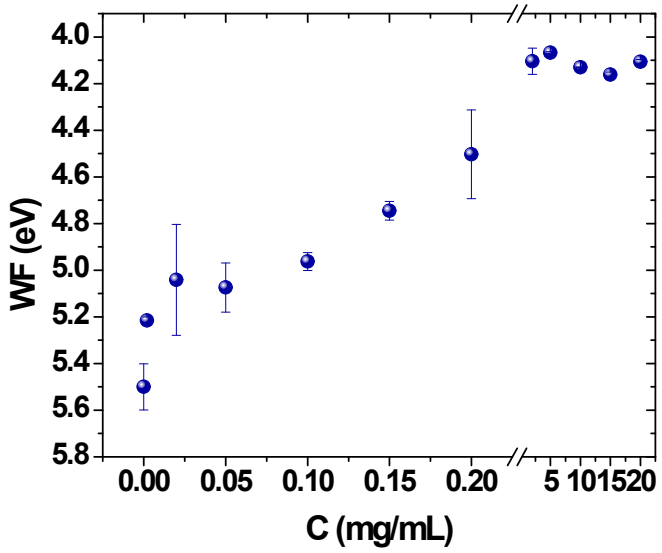

Figure S11: Work function versus doping concentrations, measured using the surface potential difference method.

The *WF* of the undoped MAPI was measured to be 5.5 eV. In the literature, this value spreads from 3.9 to 5.4 eV [2–4], therefore the *WF* measured here is too high. In spite of the use of the Faraday cage, the electrostatic noise could be responsible for the erroneous tip calibration, as the experiments were performed in the glove box. Moreover, a decrease of 1.4 eV, observed for all the doped samples, is quite large, considering that the band gap is 1.63 eV. If the *WF* change reflects the change of the E_F, then the *WF* of the heavily doped samples would be close to the electron affinity, suggesting that the undoped MAPI behaves like a strongly p-type semiconductor. This would in contradiction with the high PL intensity of the undoped sample, as well as with its low conductivity. One possibility is the presence of a surface dipole, resulting from residual Sm-species, that are observed on the AFM and SEM images (Figure 3 and S8), as well as on the XPS and ToF-SIMS depth profiles (Figure S4). Another reason could be the iodine adsorption of the golden tip used for the surface potential difference measurement during the measurement. Such

behavior was observed by Zhang *et al.*[5]. As MHPs can easily degrade upon light or moisture, one of the product of the degradation can be I_2, which can adsorb to the tip surface. This results in the increase of the *WF* of the tip. Consequently, the potential difference between the tip and the measured sample appears to be lower, resulting in the apparent *WF* of the measured sample to be lower than it really is. These two effects could result in the *WF* difference as high as 1.4 eV between the undoped and doped samples. Nevertheless, it was interesting to measure the samples with doping concentrations below 2 mg/mL. Indeed, for doping concentrations from 0.001 to 0.2 mg/mL an almost linear increase of the *WF* with the concentration is observed, suggesting a transition towards n-type semiconductor for doped samples.

UPS

When plotting the original data in the valence region, the onset of the valence band is not clear (Figure S12), especially for the highly doped samples, while for the undoped MAPI the direct extraction of the onset energy value might lead to erroneous conclusions. As pointed out by Zhang *et al.*[6], the helium lamp used as a source of UV radiation produces not only He I monochromatic line (21.22 eV), but it is also "contaminated" by satellite lines of He I^{α}, He I^{β} and He I^{γ}, with respective energies of 23.09 eV, 23.75 eV and 24.05 eV. The contribution of these satellites is not bigger than 2% and it depends on the pressure of the He lamp. Nevertheless, when the density of states is low, like in case of MAPI, even this small degree of non-monochromaticity can be an obstacle in the correct data interpretation. The amount of He I^{α}, He I^{β} and He I^{γ} radiation in this experiment was estimated to be 1.8%, 0.03% and 0.01%, respectively. In the Figure S13a. the spectrum acquired for the sample 10 mg/mL was plotted, together with the satellite lines and in

Figure S13b the result of the subsequent satellite lines removal is presented. In Figure S14 the *E w.r.t.* E_F are extracted for each doping concentration, after the satellites have been removed.

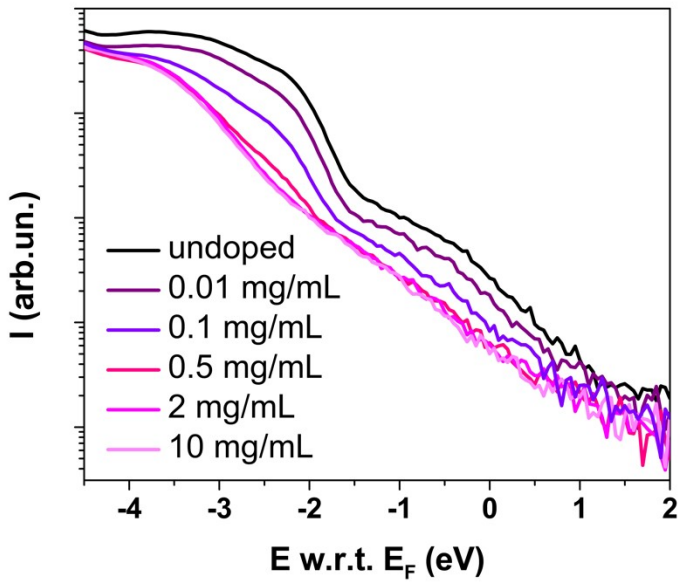

Figure S12. Original data from the UPS experiment in the valence region.

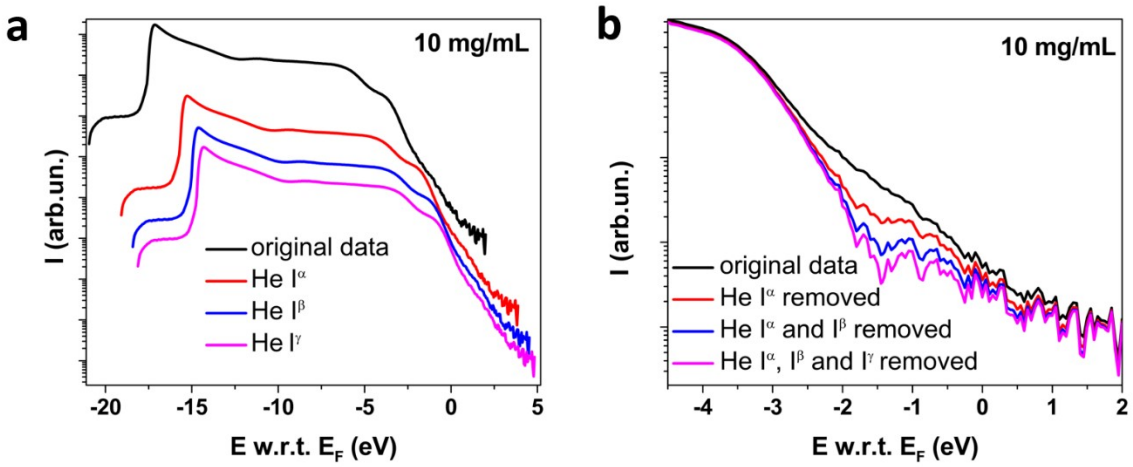

Figure S13. UPS spectra of the "10 mg/mL" sample, plotted together with the spectra resulting from the non-monochromatic radiation (a) and the same spectrum with gradually removed satellites (b).

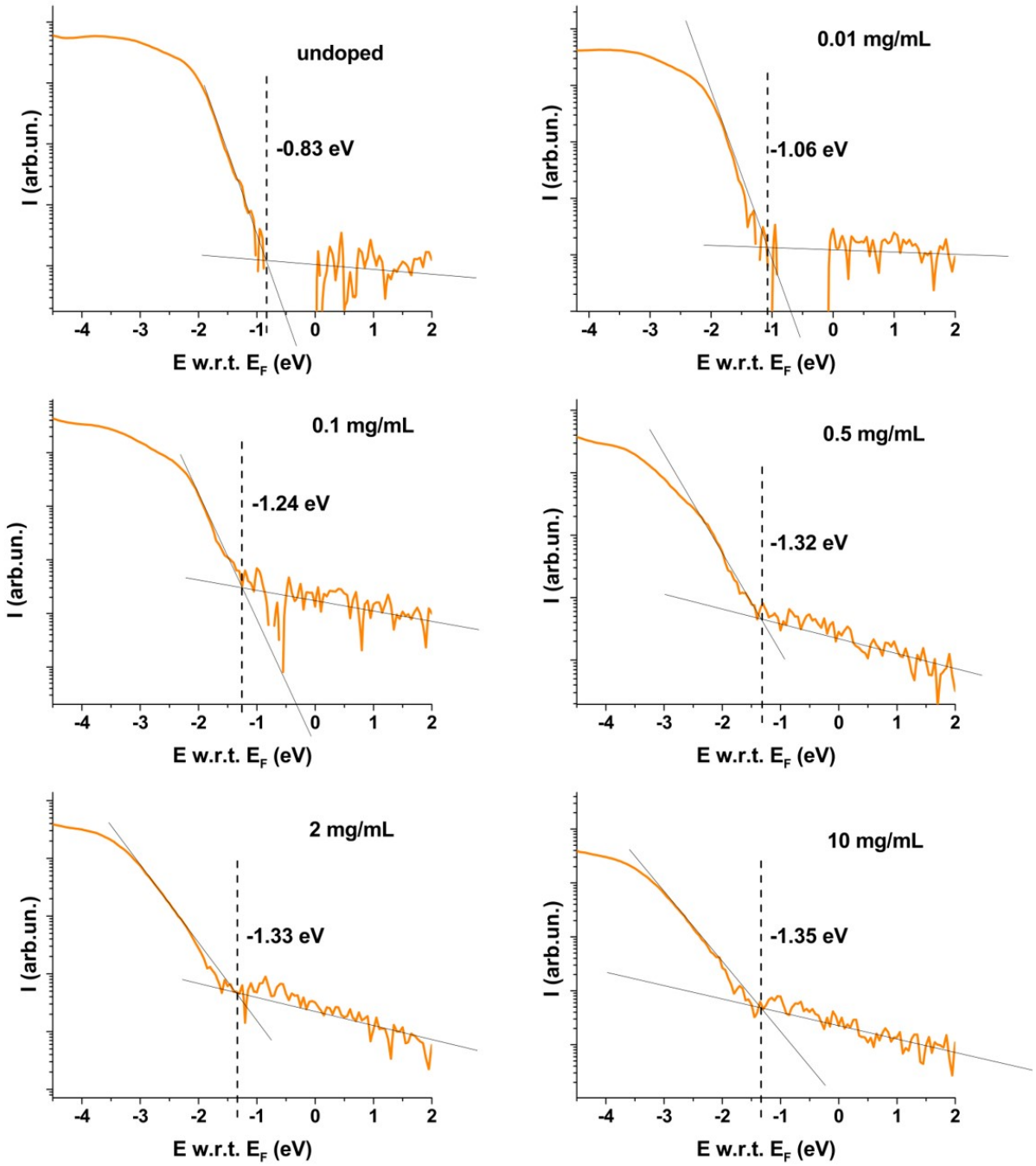

Figure S14. *E w.r.t.* E_F extracted for each doping concentration.

Impedance spectroscopy

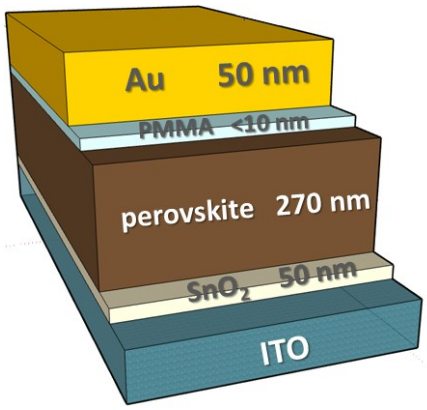

Figure S15: Sample architecture for the Mott-Schottky measurements.

Mott-Schottky analysis was performed on the undoped and doped MAPI with a thin layer of SnO_2 deposited on the ITO to ensure an ohmic contact for electrons. For the top contact, an Au electrode is used to have a blocking contact for electrons. An ultrathin (<10 nm) layer of insulating poly(methyl methacrylate) (PMMA) is intercalated between the gold electrode and perovskite, in order to reduce leakage current.

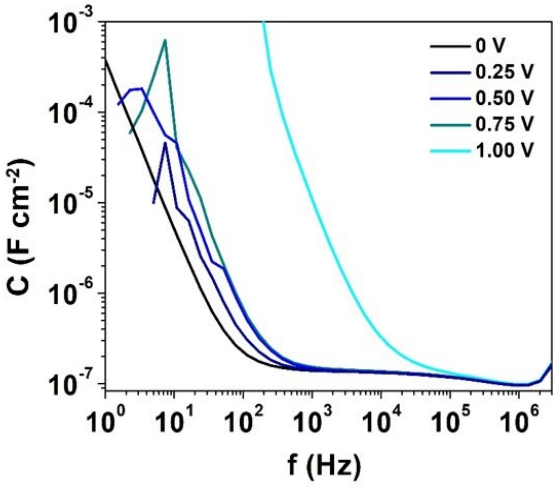

Figure S16. Capacitance as a function of frequency of the "10 mg/mL" sample.

The frequency for the Mott-Schottky measurement was chosen from the plateau region of the *C(f)* scan in order to decrease the impact of the mobile ions.

Fluxim simulations

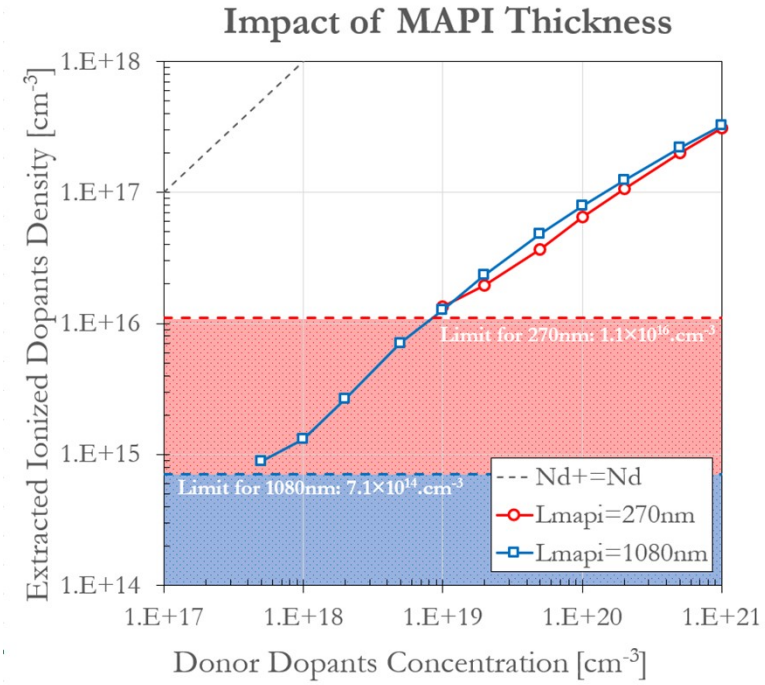

Figure S17. Simulations made for perovskites layer of two different thicknesses, 270nm and 1080nm. The Mott-Schottky analysis method limitation on thin film is due to depletion thickness greater than semiconductor thickness. The red curve with circle markers shows the impossibility to extracted dopants concentration under 1.1×10^{16} cm^{-3} for a structure of 270 nm thick. For a perovskite layer 4 times thicker (blue line with squares), the limit is of 7.1×10^{16} cm^{-3}.

Table S1. Ionized dopant concentration extracted from $1/C^2$ simulated curved versus dopant concentration as well as the solutions dopant concentration.

Nd	1×10^{18}	2×10^{18}	5×10^{18}	1×10^{19}	2×10^{19}	5×10^{19}	1×10^{20}	2×10^{20}	5×10^{20}	1×10^{21}

(cm^{-3})										
Nd^{+} (cm^{-3})	2.2×10^{16}	1.2×10^{16}	1.1×10^{16}	1.3×10^{16}	1.9×10^{16}	3.6×10^{16}	6.5×10^{16}	1.0×10^{17}	2.0×10^{17}	3.1×10^{17}
$Equ.\ Dose$ $(mg.mL^{-1})$	0.04	0.08	0.2	0.4	0.8	2	5	10	20	40

Table S2. Material Parameters Used in Simulations

$Property$	$Perovskite$ $(CH_3NH_3P_bI_3)$	$Insulator$ $(PMMA)$	ETL (S_nO_2)	$Anode$ (ITO)	$Cathode$ (Au)
$Thickness\ (nm)$	270	10	100	50	50
$Conduction\ Band\ \ (eV)$	-3.9	-1.8	-4.3	-4.7	-5.1
$Valence\ Band\ \ (eV)$	-5.5	-7.8	-8.5	-	-
$Relative\ dielectric$ $permittivity\ (\varepsilon_r)$	15	4.9	7	-	-
$Donor\ Density\ (cm^{-3})$	1×10^{17} - 1×10^{21}	-	1×10^{19}	-	-
$Acceptor\ Density\ (cm^{-3})$	1×10^{17}	-	1×10^{17}	-	-
$Electrons'\ Mobility\ (cm^2.V^{-1}.s^{-1})$	1×10^{-3}	1×10^{-5}	200		
$Holes'\ Mobility\ (cm^2.V^{-1}.s^{-1})$	1×10^{-4}	1×10^{-6}	1		
$Acceptor\ Density\ (cm^{-3})$	1×10^{17}	-	1×10^{17}	-	-

$Donor\ Activation\ Energy\ \ (eV)$	0.300	-	-	-	-
$Acceptor\ Activation\ Energy\ \ (eV)$	0.500	-	-	-	-
$Mobile\ Anion\ Density\ (cm^{-3})$	1×10^{17}	-	-	-	-
$Mobile\ Cation\ Density\ (cm^{-3})$	1×10^{17}	-	-	-	-
$Anion\ Mobility\ (cm^2.V^{-1}.s^{-1})$	5×10^{-11}	-	-	-	-
$Cation\ Mobility\ (cm^2.V^{-1}.s^{-1})$	5×10^{-14}	-	-	-	-

References

[1] J. Gomez-Bolivar, I. P. Mikheenko, R. L. Orozco, S. Sharma, D. Banerjee, M. Walker, R. A. Hand, M. L. Merroun, L. E. Macaskie, *Front. Microbiol.* **2019**, *10*, 1.

[2] M. Caputo, N. Cefarin, A. Radivo, N. Demitri, L. Gigli, J. R. Plaisier, M. Panighel, G. Di Santo, S. Moretti, A. Giglia, M. Polentarutti, F. De Angelis, E. Mosconi, P. Umari, M. Tormen, A. Goldoni, *Sci. Rep.* **2019**, *9*, 15159.

[3] K. G. Lim, H. B. Kim, J. Jeong, H. Kim, J. Y. Kim, T. W. Lee, *Adv. Mater.* **2014**, *26*, 6461.

[4] B. J. Foley, D. L. Marlowe, K. Sun, W. A. Saidi, L. Scudiero, M. C. Gupta, J. J. Choi, *Mater. Eng. Sci. Div. 2015 - Core Program. Area 2015 AIChE Annu. Meet.* **2015**, *243904*, 581.

[5] F. Zhang, F. Ullrich, S. Silver, R. A. Kerner, B. P. Rand, A. Kahn, *J. Phys. Chem. Lett.* **2019**, *10*, 890.

[6] F. Zhang, S. H. Silver, N. K. Noel, F. Ullrich, B. P. Rand, A. Kahn, *Adv. Energy Mater.*

2020, *10*, 1.